Space Confinement and Rotation Stress Induced Self-Organization of Double-Helix Nanostructure: A Nanotube Twist with a Moving Catalyst Head

Meng-Qiang Zhao, Qiang Zhang,* Gui-Li Tian, Jia-Qi Huang, and Fei Wei*

Beijing Key Laboratory of Green Chemical Reaction Engineering and Technology, Department of Chemical Engineering, Tsinghua University, Beijing 100084, China

ABSTRACT Inorganic materials with double-helix structure have attracted intensive attention due to not only their elegant morphology but also their amazing morphology-related potential applications. The investigation on the formation mechanism of the inorganic double-helix nanostructure is the first step for the fundamental studies of their materials or physical properties. Herein, we demonstrated the space confinement and rotation stress induced self-organization mechanism of the carbon nanotube (CNT)-array double helices under scanning electron microscopy by directly observing their formation process from individual layered double hydroxide flakes, which is a kind of hydrotalcite-like material composed of positively charged layers and charge-balancing interlayer anions. Space confinement is considered to be the most important extrinsic factor for the formation of CNT-array double helices. Synchronous growth of the CNT arrays oppositely from LDH flakes with space confinement on both sides at the same time is essential for the growth of CNT-array double helices. Coiling of the as-grown CNT arrays into double helices will proceed by self-organization, tending to the most stable morphology in order to release their internal rotation stress. Based on the demonstrated mechanism, effective routes were carried out to improve the selectivity for CNT-array double helices. The work provides a promising method for the fabrication of double-helix nanostructures with their two helices connected at the end by self-assembly.

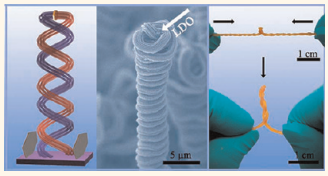

KEYWORDS: double helix · space confinement · rotation stress · carbon nanotube · layered double hydroxide

The helix is probably the most mysterious yet ubiquitous geometries that can be widely observed in nature and science, as well as human art and architectures.[1−4] Combining two congruent helices with the same axis or a translation along the axis together gives rise to a double-helix structure, which is the basic structure of deoxyribonucleic acid (DNA). Recently, inorganic materials with double-helix structure have attracted intensive attention due to not only their elegant morphology but also their amazing morphology-related potential applications.[2,4] Several synthetic methods have been established to obtain double-helical inorganic materials.[5−8] It was reported as early as 1990 that double-helical carbon fibers were synthesized by chemical vapor deposition (CVD) of acetylene on Ni particles.[5] A three-dimensional growth model based on the anisotropy of the carbon deposition among three crystal faces was proposed to illustrate their formation mechanism.[9,10] In addition, Fe particles and layered double hydroxides (LDHs) were also demonstrated to be effective catalysts for the synthesis of carbon fiber double helices.[11,12] Recently, Marito and Yamane succeeded in synthesizing double-helical Si microtubes using a Zintl compound, NaSi, as the starting material, and a formation mechanism including the trapping of Ar gas in the NaSi melts, elongation of the melt protuberances, and volume decrease driving formation of the double-helical structure was proposed.[6] Wang *et al.* achieved the chiral transformation of a single Au−Ag alloy nanowire to a double helix upon growth of a thin metal layer.[8] The formation of the metallic double helix was proposed to originate from the chirality within the original Au−Ag nanowires, which were induced to untwist upon metal deposition.[8] However, limited detailed evidence was collected to verify the related hypothetical mechanism discussed above for double-helix formation, which significantly hinders the structure control of these double-helical materials as well as the fundamental studies of their chemical or physical properties.

Carbon nanotubes (CNTs) can also be employed as promising building blocks of the helix structure to demonstrate their extraordinary electronic, mechanical, and thermal properties of one-dimensional (1D) nanomaterials.[2,13−16] Very recently, we reported that arrays of CNTs with double-helical

* Address correspondence to zhang-qiang@mails.tsinghua.edu.cn (Q.Z.); wf-dce@tsinghua.edu.cn (F.W.).

Received for review March 31, 2012 and accepted April 20, 2012.

Published online April 20, 2012
10.1021/nn301421x

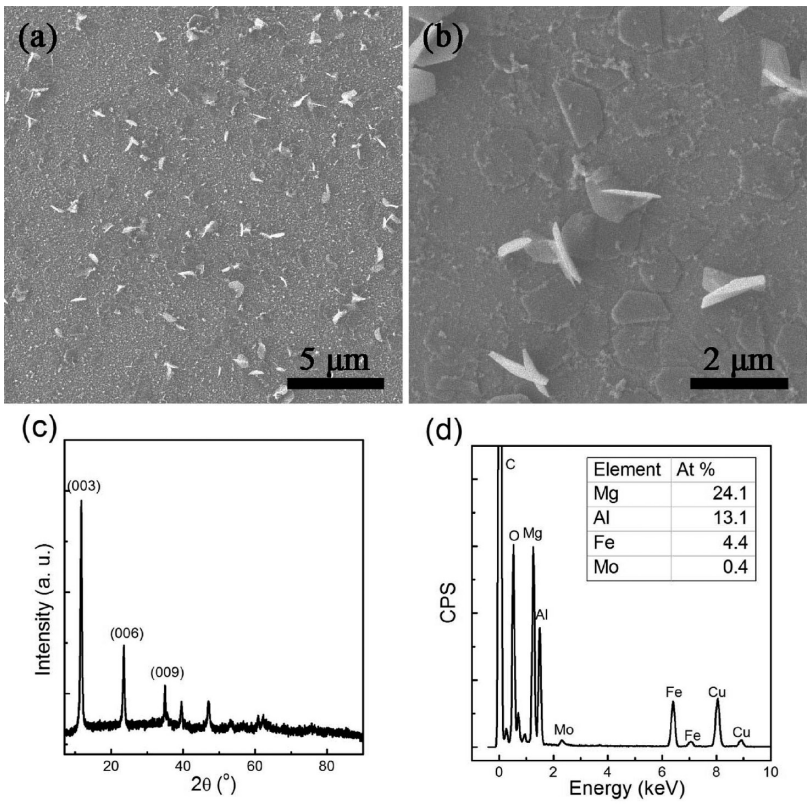

Figure 1. SEM images (a, b), XRD pattern (c), and EDXs spectrum (d) of the FeMoMgAl LDH film grown on quartz sheets.

nanostructure were obtained among the CVD growth products from LDH flakes.[7] Multiwalled, double-walled, and single-walled CNT-array double helices were all successfully fabricated by selecting proper LDH flakes with tunable metal catalysts.[7,17−19] However, the poor selectivity of these double helices compared with the CNT bundles and the lack of orientation of the as-synthesized CNT-array double helices seriously impeded their property and application explorations. Investigation of the formation mechanism to reveal how a CNT-array double helix is formed from a LDH flake is considered to be the first step to overcome such difficulties. In the previous studies, a pile of stacked LDH aggregates was employed as the catalyst precursor. It is impossible to observe the evolution process of an individual CNT-array double helix from a LDH flake and thus obtain its formation mechanism directly. Recent advances on LDH film preparation provide the possibility that LDH flakes can be uniformly and vertically distributed on the surface of various substrates with a tunable density.[20−22] We have previously succeeded in synthesizing short aligned single-walled CNTs (SWCNTs) with uniform length distribution using such perpendicular FeMoMgAl LDH films.[22] Herein, a single-layered FeMoMgAl LDH film with the flakes sparsely distributed on a quartz substrate as the catalyst precursor was used to form CNT-array double helices. This made it possible to take a look at the formation process of a CNT-array double helix from an individual LDH flake and, thus, demonstrated the formation mechanism of the CNT-array double helix.

RESULTS AND DISCUSSIONS

The morphology of the as-prepared LDH film is shown in Figure 1a and b. The as-synthesized hexagonal LDH flakes were uniformly and sparsely distributed on the surface of the quartz sheet. They have a distance of several micrometers between each other, which is similar to the diameter size of the CNT-array double helices.[7,17,18] The powder X-ray diffraction (XRD) (Figure 1c) pattern of the LDH flakes collected from the quartz sheets revealed that the as-synthesized FeMoMgAl LDH flakes were well crystallized and had lattice parameters of a = 0.304 nm and c = 2.276 nm. The formula of the FeMoMgAl flakes can be represented as $[Mg_{0.58}Al_{0.31}Fe_{0.11}(OH)_2][(CO_3)_{0.20}(MoO_4)_{0.01}]\cdot mH_2O$ based on the results of the energy dispersive X-ray spectrometry (EDXs) of the LDH flakes (Figure 1d).

Growth of the CNT-array double helices was carried out using a catalytic thermal CVD with the as-prepared FeMoMgAl LDH films as the catalyst precursor. Samples with different growth durations (2, 15, and 60 min) were collected separately and characterized by scanning electron microscopy (SEM) to observe the entire growth process of the CNT-array double helices (Figure 2). After a growth duration of 2 min, short aligned CNT

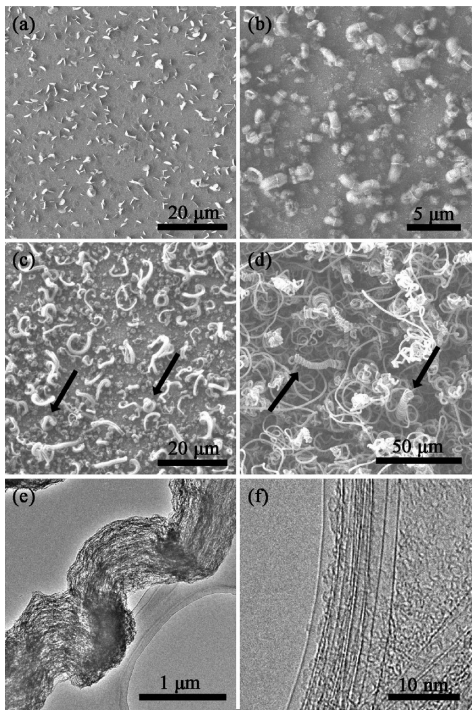

Figure 2. SEM images of (a) the FeMoMgAl LDH film grown on a quartz sheet and the as-grown CNTs after CVD of ethylene for (b) 2, (c) 15, and (d) 60 min. (e) TEM and (f) high-resolution TEM images of the as-grown CNTs after CVD of ethylene for 60 min.

arrays with a length around 1 μm grown on both sides of the LDH flakes can be observed, indicating the initial growth stage of the CNT-array double helices (Figure 2b). With a prolonged growth duration of 15 min, the as-grown products were mainly composed of CNT bundles with a diameter of 1 μm and a length larger than 10 μm. However, it is also noticed that several primary CNT-array double helices with one or two pitches can also be observed, as indicated by the black arrows in Figure 2c. When further increasing the growth duration to 60 min, both CNT bundles and CNT-array double helices with a length of tens of micrometers were observed (Figure 2d). We conclude that detailed characterization of the growth process of the CNT-array double helices with a growth duration within 15 min is most suitable to obtain the growth mechanism. The transmission electron microscopy (TEM) image of a curved CNT bundle from the growth duration of 60 min shows that the as-grown CNTs are well aligned. A high-resolution TEM image (Figure 2f) and Raman spectra of the CNT samples (Figure 3) revealed that the as-grown CNTs were mainly SWCNTs. The I_D/I_G ratios for the CNT samples were 0.11, 0.21, and 0.18, which correspond to 2, 15, and 60 min growth, respectively. Note that the I_D/I_G ratios for the SWCNT-array double helices are much larger than the SWCNTs in other morphologies, including entangled SWCNTs,[23] SWCNT arrays,[24] and SWCNT bundles.[25] This indicates that the SWCNT-array double helices had a much larger defect density. The formation of single -helical CNT was accompanied by a concomitant insertion of pentagon and heptagon pairs into the hexagonal sheet of the growing nanotube, leading to a high defect density.[26,27] Herein, coiling of the SWCNT arrays into a double-helical structure also corresponded to a high defect density of the SWCNTs, although a much different formation mechanism was proposed.

There were three different kinds of relative positions when the as-obtained LDH flakes attached to the quartz substrate in the as-prepared LDH film (Figure 4a−c). The calcination and reduction of these LDH flakes led to the formation of their corresponding layered double oxide (LDO) flakes without any change in their morphology and location.[17,23,28] A part of the LDH flakes grew horizontally to the surface of the quartz sheet (Figure 4a). The SEM image of the sample after a 2 min growth showed that only entangled CNTs were available from these horizontal LDH flakes due to the strong interaction between the LDH flakes and the quartz substrate (Figure 4d). Some of the LDH flakes grew slantwise to the surface of the quartz substrate. Upon the decomposition of C_2H_4, aligned CNTs can grow from both sides of the LDH flakes. Since the LDH flakes synthesized were considered to be a monocrystal and the metal cations in the LDH flakes were dispersed *at an atomic level*,[17,29] it was suspected that the two sides of the LDH flakes exhibited the same reactivity for the growth of CNTs. During the initial growth stage, space confinement between the substrate and LDH flakes hindered further growth of the aligned CNTs on the acute-angle side of these LDH flakes. However, the aligned CNTs on the other side kept growing, leading to the different lengths of the CNT arrays on both sides of the slantwise LDH flakes (Figure 4e). Some LDH flakes grew perpendicularly to the surface of the substrate (Figure 4c). The growth of CNT arrays on both sides of these LDH flakes can proceed freely without any space confinement during the initial growth stage, which led to their similar length (Figure 4f).

When the growth duration was prolonged to 15 min, it was observed that the as-grown CNT arrays on the obtuse side of the slantwise LDH flakes continued to grow. However, the growth of CNT arrays on the acute-angle side of the slantwise LDH flakes was inhibited. As a result, long CNT bundles with the corresponding LDO flakes on one side were formed, as revealed by the white arrows in Figure 5a. As for the growth of CNT arrays from the perpendicular LDH flakes, three different situations were observed. If the CNT arrays grown on both sides of the flakes were free of space confinement, long CNT bundles with the corresponding LDO flakes located at the middle of the bundle were formed (Figure 5b). If the space confinement occurred on one side of the LDH flakes from neighboring as-grown CNTs shortly after the growth of CNT arrays, while the CNT

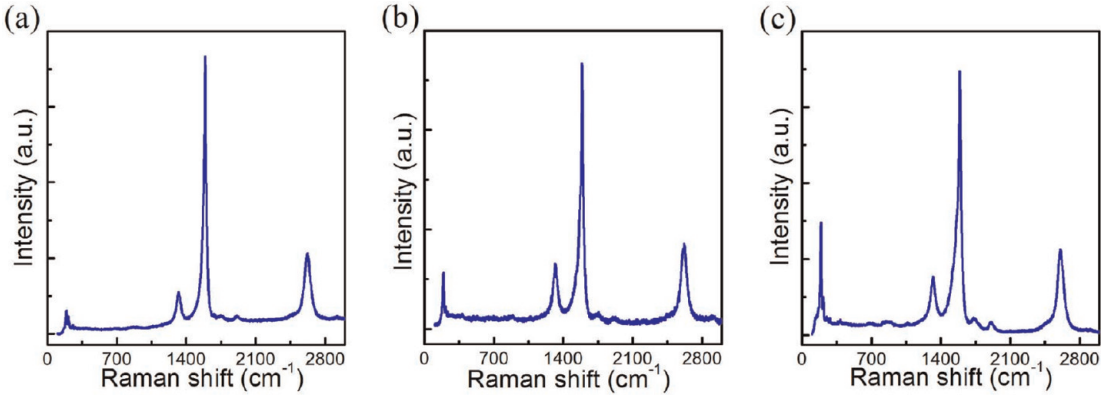

Figure 3. Raman spectra of the as-grown CNTs from the FeMoMgAl LDH films after CVD of ethylene for (a) 2, (b) 15, and (c) 60 min.

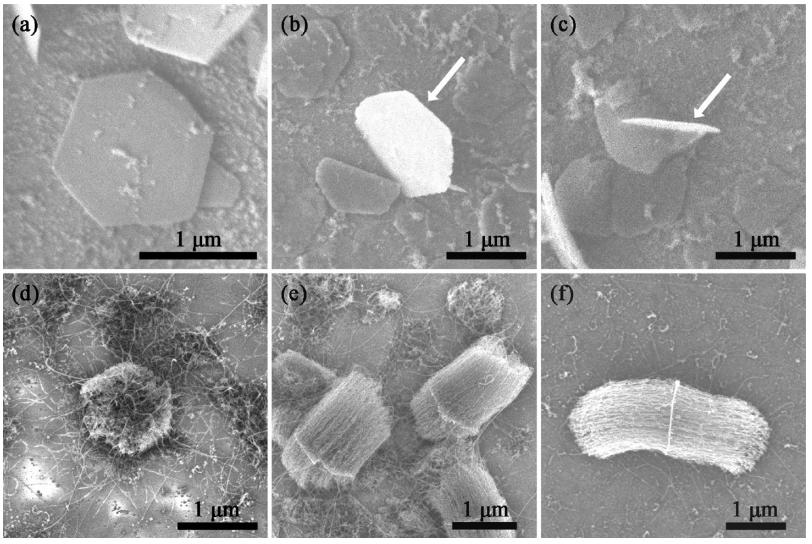

Figure 4. SEM images of the FeMoMgAl LDH flakes grown (a) horizontally, (b) slantwise, and (c) perpendicularly to the surface of quartz substrate and (d−f) their corresponding as-grown CNTs after CVD of ethylene for 2 min.

arrays on the other side can still grew freely, this also led to the formation of long CNT bundles with the corresponding LDO flakes located on the side where the space confinement occurred (Figure 5c). Only if the as-grown CNT arrays on both sides of the LDH flakes met space confinement shortly after the start of the reaction can the formation of the CNT−array double helix with a LDO flake head be observed, as shown in Figure 5d. However, when the distance of the space confinement was too large, the situation can be considered the same as that free of space confinement (Figure 5b). In addition, it should be noted that because the as-grown CNT-array double helices all had a closely coiled morphology with similar pitch angle, the diameter of the CNT-array double helices was considered to be determined by the diameter of the composed CNT stands and, therefore, by the size of the original LDO flakes.

Usually, a driving force for the twisting is highly required for the inherent simultaneous shift and rotation between the building blocks. For instance, during the dislocation-dominated physical deposition, a screw-like dislocation in the nanowire/tube trunks provided a rapid growth driving force and directed the helical rotating epitaxial growth of branches of hierarchical helical PdS[30] or PdSe[31] nanostructures. The chiral organogels,[32] peptides,[33,34] DNA,[35] lipid tubules,[36] cholate,[37] and micelles[38] served as molds to replicate their helical structures with inorganic materials. When the nanocrystal building blocks were self-assembled or continuously grown into nanoarchitectures, some surface ligands, such as poly(aspartate),[39] EPG-b-DHPOVAEE,[40] can absorb on the surface of nuclei of a nanoparticle to inhibit the crystal growth along specific directions and promote the spiral growth of anisotropic helical $CaCO_3$[39] and $BaCO_3$.[40] The inversion of the lamellar twisting chirality of microbial copolymers induced by surface stress from left-handed to right-handed *via* copolymerization or blending leads to the formation of chiral polymers.[41,42] Herein, the driving force was attributed to the tendency of releasing the internal rotation stress of the rotated CNT arrays oppositely and synchronously

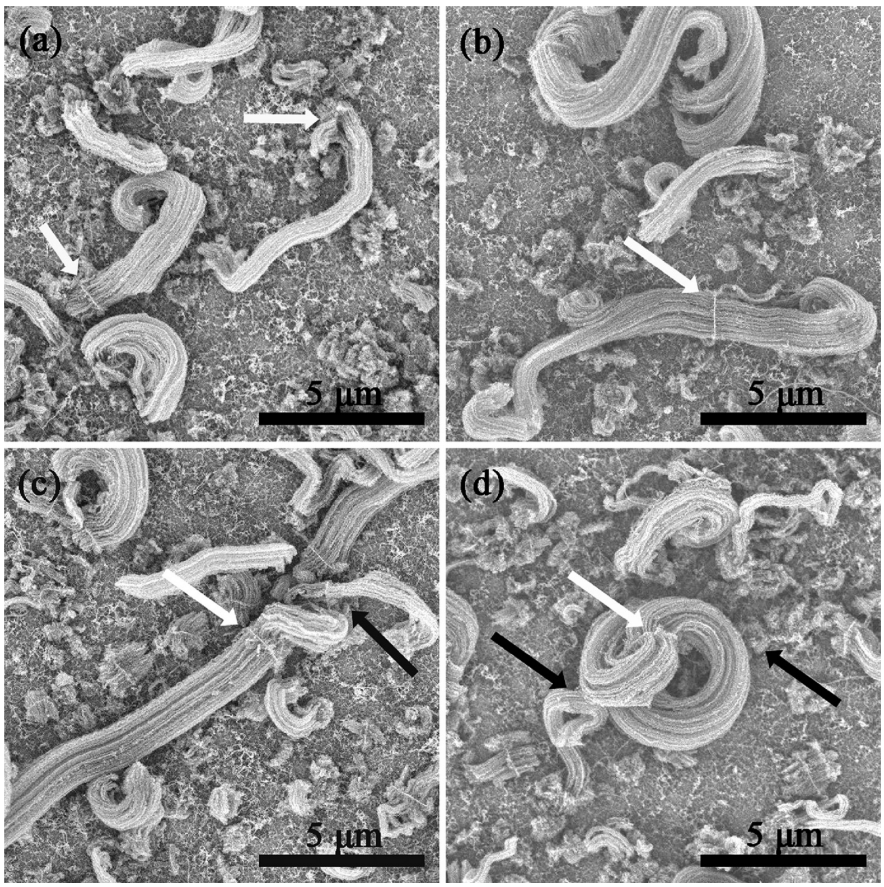

Figure 5. SEM images of long CNT bundles grown from (a) slantwise LDH flakes, (b) perpendicular LDH flakes without space confinement, and (c) perpendicular LDH flakes with space confinement at one direction of the CNT growth. (d) SEM image of the CNT double helix grown from perpendicular LDH flakes with space confinement at both directions of the CNT growth. The LDH flakes are indicated by white arrows, while the positions where the space confinements occurred are indicated by black arrows.

grown on a LDO flake. The CNT is a typical chiral nanomaterial that can be viewed as having a screw dislocation along the axis. Although CNTs are produced in a seemingly random distribution of diameters and chiral symmetry in most cases, Ding *et al*. illustrated that the growth rate of CNTs is shown to be proportional to the Burgers vector of such dislocation and therefore to the chiral angle.[43] The direct observation result of individual CNT growth by field emission microscopy indicates that CNTs often rotate axially during growth. The CNT turned *ca.* 180 times during its 11 min growth, and the rotation proceeds by discrete steps with about *ca.* 24 per rotation, half the number of atoms on the circumferences of common SWCNTs.[44] The TEM characterization of MWCNT catalysts by Behr *et al*. also confirmed the random small-angle (1−3°) rotation misorientations between adjacent sections along catalyst crystals, indicating that the CNTs exert stresses that rotate, twist, and bend small sections of the catalyst during growth, which can be considered as an evidence of the rotation of CNTs during the growth on the other hand.[45] Note that the CNTs grown from the LDH catalysts had a tortuous morphology rather than a straight form (Figure 6a−c). Thus, it is suspected that the formation of the internal rotation stress can be considered as a consequence of the fact that the rotation of individual CNTs was impeded by neighboring CNTs in the as-grown CNT arrays. When two CNT strands oppositely grow on a catalyst flake with their two tips under space confinement, the unmatched precipitation of a large amount of CNTs from the metal catalyst particle distributed on the flake causes strong internal rotation stresses. As shown in Figure 6a, for the CNT arrays that did not twist into a double helix, the rotation of the arrays along the axis can always be observed. A rotation angle of 90° along the axis of the CNT arrays was observed when it proceeds a distance of 5 μm, indicating the existence of serious internal rotation stresses. It is interesting to note that the two CNT arrays oppositely grown from a LDO flake always exhibited the same handed rotation (Figure 6b), which is of paramount importance for the successful self-assembly of CNT-array double helices. However, no obvious rotation of the individual CNT array can be found in the CNT-array double helix, which indicates that the internal rotation stress has been released after the formation of the double-helix structure. A rubber band with a node was taken as an

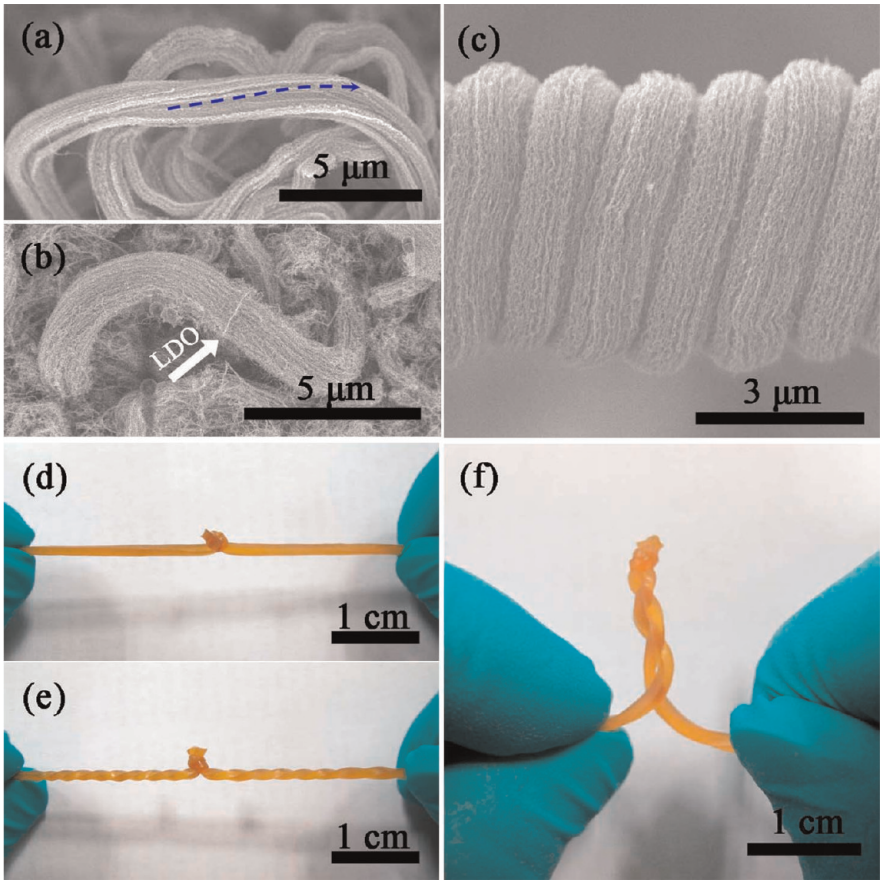

Figure 6. SEM image showing (a) a long CNT bundle with obvious rotation, (b) two CNT bundles grown oppositely from a LDO flake with the same right-handed rotation, and (c) the nonrotation of the CNT bundles in the CNT-array double helix. (d–f) Photo images showing evolution process of the self-organization of a twisted rubber band with a node into a double-helical structure.

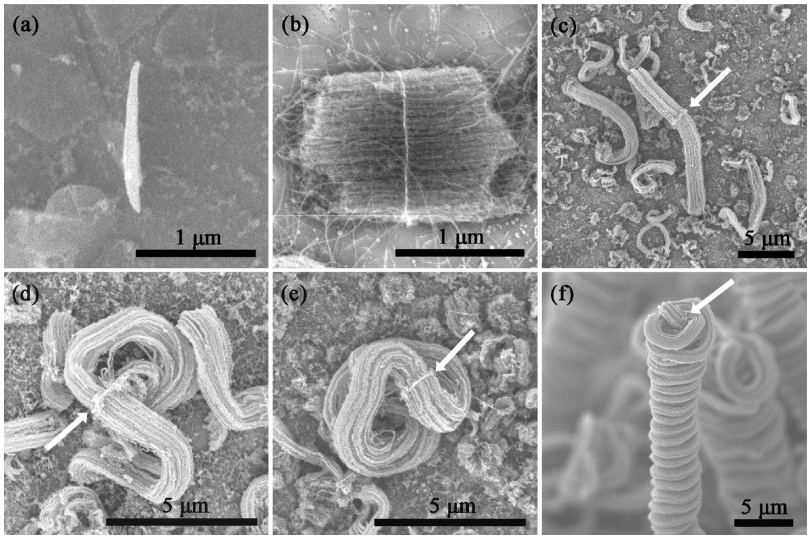

Figure 7. SEM images showing the formation process of CNT double helix: (a) perpendicular LDH flake on the surface of the substrate; (b) morphology of the as-grown CNT arrays after (b) 2 min, (c–e) 15 min, and (f) 60 min growth.

example to get a better understanding, as shown in Figure 6d–f and movie S1 in the Supporting Information. The two ends of the rubber band were twisted in opposite directions first to give rise to the same handed rotation of the two parts of the rubber band at both sides of the node. When approaching the two ends of the twisted rubber band together, which is considered as the other form of space confinement for

the two twisted fibers, a kind of double-helical structure with two parts of the rubber band connected by the node will be self-organized, and the rotation stresses of the rubber band were much released according to the changes of its rotation angle (Figure 6e and f). Therefore, it is suspected that twisting of the CNT arrays into a double-helical structure with the catalyst flake as the head is the best way to release the internal stress and minimize the energy. The symmetry growth and self-rotation of aligned CNTs with different expending directions under confinement lead to changes of configuration. The continuous precipitation of CNTs under space confinement provides the driving force for *in situ* twisting, and the active site is always centered at the catalyst head. It is also noticed from movie S1 that self-organization of two fibers with left-handed self-rotation connected by a node leads to the formation of a double-helix structure with two right-handed helices, while self-organization of two fibers with right-handed self-rotation connected by a node leads to the formation of a double-helix structure with two left-handed helices. This indicates that the chirality of the self-organized double helix depends on the self-rotation direction of the two original fibers. It is observed that the CNT-array double helices showed no chirality selectivity; thus the rotation direction of the as-grown CNT arrays was suspected to be stochastic. Selective fabrication of right- or left-handed CNT-array double helices still requires further study of the reason for the self-rotation of the as-grown CNT arrays and their rotation direction control.

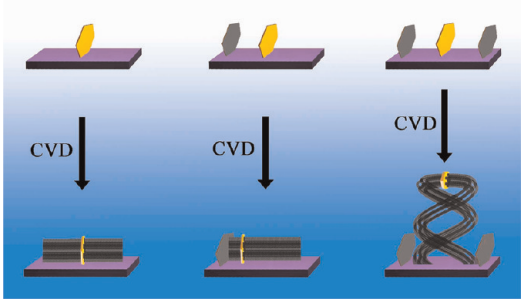

Scheme 1. Schematic illustration showing the three different evolution processes for CNT array growth from both sides of a LDH flake (space confinement is indicated by the gray flakes).

Because the organization of CNT-array double helices is a spontaneous behavior, space confinement is considered to be the most important extrinsic factor that plays an important role in the morphology of the as-grown CNT arrays from the LDH flakes. As shown in Scheme 1, the process of space confinement formation on a flake is the key step in the initial growth of double-helical CNT arrays. The formation of a long CNT bundle with a LDO flake at the middle can be achieved when the confinement was free. If the space confinement occurs only on one side of the flake shortly after the CVD growth, long CNT bundles with a LDO flake located at the end where the space confinement occurred will be formed. However, space confinement on both sides of the LDH flake can facilitate the self-organization of a CNT-array double helix. The space confinement can originate from the substrate, neighboring LDO flakes, or CNTs. It should be noted that the location of the space confinement discussed here is on the same order of magnitude as the diameter of the as-obtained CNT-array double helices. As show in Figure 7a–f, aligned CNTs can grow synchronously from both sides of the perpendicular LDO flakes. Continuous growth of the CNT arrays will cause a propulsive force to lift up the LDO flakes. A kind of internal stress is formed due to the rotation of the CNTs, and the as-grown aligned CNTs with the same-handed rotation will coil on themselves in order to release the internal stress and achieve a more stable morphology by self-organization, which finally forms the CNT-array double helix.

On the basis of the above-mentioned formation mechanism of CNT-array double helices, it is believed that the formation of CNT-array double helices from other kinds of catalyst flakes can also be achieved if the

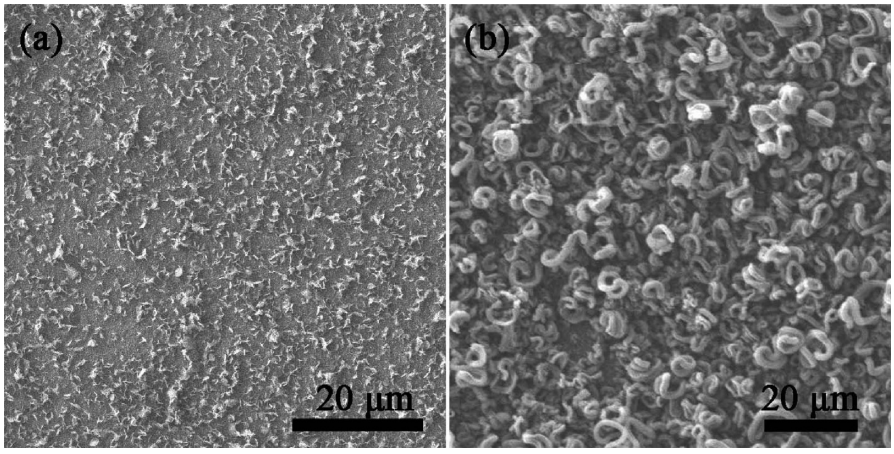

Figure 8. SEM images of (a) the densified LDH film and (b) its as-grown CNTs with improved selectivity of CNT-array double helices.

essentials mentioned above are satisfied. For instance, the very recent report from Terrones' group demonstrated that double-helical multiwalled CNT array structures were successfully fabricated with lamellar SiO_x particles-supported Fe nanoparticles as the catalyst flakes.[46] In addition, it is suspected that proper increasing density of the perpendicular LDH film will enhance the probability of space confinement occurring on both sides of the LDO flakes and, thus, improve the selectivity of the CNT-array double helices. This has been demonstrated experimentally by using densified LDH film for the CVD growth. As shown in Figure 8, when the density of LDH flakes was increased 10 times (compared with the LDH film shown in Figure 2a), the density of the CNT-array double helix increased around 100 times, indicating the selectivity was much improved. However, further improvement of the selectivity of the CNT-array double helices requires the alignment of the perpendicular LDH flakes with controlled density, which is still a great challenge for material synthesis.

CONCLUSIONS

The evolution process of the CNT-array double helices was demonstrated by direct observation under SEM, which contributed to the experimental evidence for the space confinement and rotation stress induced self-organization mechanism of CNT arrays twisted with a catalyst head. Space confinement is considered to be the most important extrinsic factor for the formation of CNT-array double helices. Synchronous growth of the CNT arrays oppositely from LDH flakes with space confinement on both sides at the same time is essential for the growth of CNT-array double helices. Coiling of the as-grown CNT arrays into double helices will proceed with self-organization, tending to the most stable morphology in order to release the internal rotation stress in the two CNT arrays on both sides of the LDO flake, which always had the same handed rotation. It is anticipated that high selectivity and even orientation of the CNT-array double helices will be available if the LDH flake catalysts are vertically or inclined well aligned on the substrates with tunable density. The as-obtained CNTs can even be organized into complex hierarchical nanoarchitectures if the LDH catalyst has a site-selective and alignment-mediated arrangement. Furthermore, if the reason and direction of the self-rotation of the as-grown CNT arrays can be well studied and controlled, right- and left-handed double helices will be available during the self-assembly process.

EXPERIMENTAL METHODS

Preparation of the LDH Film. The FeMoMgAl LDH films were prepared using a urea-assisted co-precipitation reaction with quartz sheets as the substrates. In a typical procedure, $Mg(NO_3)_2 \cdot 6H_2O$, $Al(NO_3)_3 \cdot 9H_2O$, $Fe(NO_3)_3 \cdot 9H_2O$, $Na_2MoO_4 \cdot 2H_2O$, and urea were dissolved in 250.0 mL of deionized water with $[Mg^{2+}] + [Al^{3+}] = 0.15$ mol/L, n(Mg):n(Al):n(Fe):n(Mo) = 2:1:0.4:0.04, [urea] = 3.0 mol/L. Then, quartz sheets with a size of *ca.* 1 cm^2, which were treated by ultrasonication in ethanol for 10 min, were added to the solution. The prepared solution with quartz sheets was then heated to 94 °C and kept for 12 h in a 500 mL flask (equipped with a reflux condenser) under ambient atmosphere. After the completion of the LDH film growth, the quartz sheets were taken out of the flask and rinsed with deionized water thoroughly. Finally, the quartz sheets were dried at 100 °C in an oven for 12 h for further characterizations and growth of CNTs. The densified LDH film was prepared using a similar procedure except that the quartz sheets, which were first treated by ultrasonication in ethanol for 10 min and then in HCl aqueous solution for 10 min subsequently, served as the substrates.

Growth of CNTs. The prepared FeMoMgAl LDH films on quartz sheets were placed at the center of a horizontal quartz tube inserted into a furnace at atmospheric pressure. Then the furnace was heated under flowing Ar (600 mL/min). On reaching 850 °C, H_2 (50 mL/min) was introduced into the reactor, 5 min before the introduction of C_2H_4 (6 mL/min) into the reactor. The growth of CNTs was maintained for a designated duration (2, 15, and 60 min) at 850 °C before the furnace was cooled to room temperature under Ar flow. After that, the samples with different growth durations were collected for further characterizations.

Characterizations. The as-prepared samples were characterized using a JSM 7401F (JEOL Ltd., Tokyo, Japan) scanning electron microscopy operated at 3.0 kV and a JEM 2010 (JEOL Ltd., Tokyo, Japan) transmission electron microscopy operated at 120.0 kV. The specimens for TEM observation were prepared using a common sonication method. Energy-dispersive X-ray spectrometer analysis was performed using a JSM-7401F apparatus with the analytical software INCA, and the accelerating voltage applied was 15.0 kV. X-ray diffraction patterns were recorded on a Rigaku D/max-RB diffractometer at 40.0 kV and 120 mA with Cu Kα radiation. The EDXs and XRD characterizations were performed on FeMoMgAl LDH powders collected from the vertical LDH film to avoid the influence of the quartz substrate. Raman spectra were obtained with He−Ne laser excitation at 633 nm using a Renishaw RM2000.

Conflict of Interest: The authors declare no competing financial interest.

Acknowledgment. This work was supported by National Basic Research Program of China (973 Program, 2011CB932602) and Natural Scientific Foundation of China (Key Program, Nos. 20736004 and 20736007).

Supporting Information Available: A movie showing the self-organization of two twisted fibers connected by a node into the double-helix structure and the process toward its left-handed and right-handed selectivity. This material is available free of charge *via* the Internet at http://pubs.acs.org.

REFERENCES AND NOTES

1. Albrecht, M. "Let's Twist Again" - Double-Stranded, Triple-Stranded, and Circular Helicates. *Chem. Rev.* **2001**, *101*, 3457–3497.
2. Yang, M.; Kotov, N. A. Nanoscale Helices From Inorganic Materials. *J. Mater. Chem.* **2011**, *21*, 6775–6792.
3. Imai, H.; Oaki, Y. Emergence of Helical Morphologies with Crystals: Twisted Growth under Diffusion-Limited Conditions and Chirality Control with Molecular Recognition. *CrystEngComm* **2010**, *12*, 1679–1687.

4. Su, D. S. Inorganic Materials with Double-Helix Structures. *Angew. Chem., Int. Ed.* **2011**, *50*, 4747–4750.
5. Motojima, S.; Kawaguchi, M.; Nozaki, K.; Iwanaga, H. Growth of Regularly Coiled Carbon Filaments by Ni Catalyzed Pyrolysis of Acetylene, and Their Morphology and Extension Characteristics. *Appl. Phys. Lett.* **1990**, *56*, 321–323.
6. Morito, H.; Yamane, H. Double-Helical Silicon Microtubes. *Angew. Chem., Int. Ed.* **2010**, *49*, 3638–3641.
7. Zhang, Q.; Zhao, M. Q.; Tang, D. M.; Li, F.; Huang, J. Q.; Liu, B.; Zhu, W. C.; Zhang, Y.-H.; Wei, F. Carbon-Nanotube-Array Double Helices. *Angew. Chem., Int. Ed.* **2010**, *49*, 3642–3645.
8. Wang, Y.; Wang, Q.; Sun, H.; Zhang, W.; Chen, G.; Wang, Y.; Shen, X.; Han, Y.; Lu, X.; Chen, H. Chiral Transformation: From Single Nanowire to Double Helix. *J. Am. Chem. Soc.* **2011**, *133*, 20060–20063.
9. Motojima, S.; Kawaguchi, M.; Nozaki, K.; Iwanaga, H. Preparation of Coiled Carbon-Fibers by Catalytic Pyrolysis of Acetylene, and Its Morphology and Extension Characteristics. *Carbon* **1991**, *29*, 379–385.
10. Motojima, S.; Chen, Q. Q. Three-Dimensional Growth Mechanism of Cosmo-Mimetic Carbon Microcoils Obtained by Chemical Vapor Deposition. *J. Appl. Phys.* **1999**, *85*, 3919–3921.
11. Liu, J.; Zhang, X.; Zhang, Y. J.; Chen, X. H.; Zhu, J. Nano-Sized Double Helices and Braids: Interesting Carbon Nanostructures. *Mater. Res. Bull.* **2003**, *38*, 261–267.
12. Zhang, L.; Li, F. Helical Nanocoiled and Microcoiled Carbon Fibers as Effective Catalyst Supports for Electrooxidation of Methanol. *Electrochim. Acta* **2010**, *55*, 6695–6702.
13. Huang, J. Q.; Zhang, Q.; Wei, F. Coiled Carbon Nanotubes. *Prog. Chem.* **2009**, *21*, 637–643.
14. Hanus, M. J.; Harris, A. I. Synthesis, Characterisation and Applications of Coiled Carbon Nanotubes. *J. Nanosci. Nanotechnol.* **2010**, *10*, 2261–2283.
15. Tessonnier, J. P.; Su, D. S. Recent Progress on the Growth Mechanism of Carbon Nanotubes: A Review. *ChemSusChem* **2011**, *4*, 824–847.
16. Zhang, Q.; Huang, J. Q.; Zhao, M. Q.; Qian, W. Z.; Wei, F. Carbon Nanotube Mass Production: Principles and Processes. *ChemSusChem* **2011**, *4*, 864–889.
17. Zhao, M. Q.; Zhang, Q.; Zhang, W.; Huang, J. Q.; Zhang, Y.; Su, D. S.; Wei, F. Embedded High Density Metal Nanoparticles with Extraordinary Thermal Stability Derived from Guest-Host Mediated Layered Double Hydroxides. *J. Am. Chem. Soc.* **2010**, *132*, 14739–14741.
18. Zhao, M. Q.; Huang, J. Q.; Zhang, Q.; Nie, J. Q.; Wei, F. Stretchable Single-Walled Carbon Nanotube Double Helices Derived from Molybdenum-Containing Layered Double Hydroxides. *Carbon* **2011**, *49*, 2148–2152.
19. Zhao, M.-Q.; Zhang, Q.; Huang, J.-Q.; Wei, F. Hierarchical Nanocomposites Derived from Nanocarbons and Layered Double Hydroxides - Properties, Synthesis, and Applications. *Adv. Funct. Mater.* **2012**, *22*, 675–694.
20. Guo, X.; Zhang, F.; Evans, D. G.; Duan, X. Layered Double Hydroxide Films: Synthesis, Properties and Applications. *Chem. Commun.* **2010**, *46*, 5197–5210.
21. Guo, X.; Zhang, F.; Xu, S.; Evans, D. G.; Duan, X. Preparation of Layered Double Hydroxide Films with Different Orientations on the Opposite Sides of a Glass Substrate by *in Situ* Hydrothermal Crystallization. *Chem. Commun.* **2009**, *44*, 6836–6838.
22. Zhao, M. Q.; Tian, G. L.; Zhang, Q.; Huang, J.-Q.; Nie, J.-Q.; Wei, F. Preferential Growth of Short Aligned, Metallic-Rich Single-Walled Carbon Nanotubes from Perpendicular Layered Double Hydroxide Film. *Nanoscale* **2012**, *4*, 2470–2477.
23. Zhao, M. Q.; Zhang, Q.; Jia, X. L.; Huang, J. Q.; Zhang, Y. H.; Wei, F. Hierarchical Composites of Single/Double-Walled Carbon Nanotubes Interlinked Flakes from Direct Carbon Deposition on Layered Double Hydroxides. *Adv. Funct. Mater.* **2010**, *20*, 677–685.
24. Hata, K.; Futaba, D. N.; Mizuno, K.; Namai, T.; Yumura, M.; Iijima, S. Water-Assisted Highly Efficient Synthesis of Impurity-Free Single-Walled Carbon Nanotubes. *Science* **2004**, *306*, 1362–1364.
25. Pint, C. L.; Pheasant, S. T.; Pasquali, M.; Coulter, K. E.; Schmidt, H. K.; Hauge, R. H. Synthesis of High Aspect-Ratio Carbon Nanotube "Flying Carpets" from Nanostructured Flake Substrates. *Nano Lett.* **2008**, *8*, 1879–1883.
26. Ihara, S.; Itoh, S.; Kitakami, J. Helically Coiled Cage Forms of Graphitic Carbon. *Phys. Rev. B* **1993**, *48*, 5643–5647.
27. Amelinckx, S.; Zhang, X. B.; Bernaerts, D.; Zhang, X. F.; Ivanov, V.; Nagy, J. B. A Formation Mechanism for Catalytically Grown Helix-Shaped Graphite Nanotubes. *Science* **1994**, *265*, 635–639.
28. Zhao, M. Q.; Zhang, Q.; Huang, J. Q.; Nie, J. Q.; Wei, F. Layered Double Hydroxides as Catalysts for the Efficient Growth of High Quality Single-Walled Carbon Nanotubes in A Fluidized Bed Reactor. *Carbon* **2010**, *48*, 3260–3270.
29. Evans, D. G.; Slade, R. C. T. Structural Aspects of Layered Double Hydroxides. *Struct. Bonding (Berlin)* **2006**, *119*, 1–87.
30. Bierman, M. J.; Lau, Y. K. A.; Kvit, A. V.; Schmitt, A. L.; Jin, S. Dislocation-Driven Nanowire Growth and Eshelby Twist. *Science* **2008**, *320*, 1060–1063.
31. Zhu, J.; Peng, H. L.; Marshall, A. F.; Barnett, D. M.; Nix, W. D.; Cui, Y. Formation of Chiral Branched Nanowires by The Eshelby Twist. *Nat. Nanotechnol.* **2008**, *3*, 477–481.
32. Sone, E. D.; Zubarev, E. R.; Stupp, S. I. Supramolecular Templating of Single and Double Nanohelices of Cadmium Sulfide. *Small* **2005**, *1*, 694–697.
33. Guha, S.; Drew, M. G. B.; Banerjee, A. Construction of Helical Nanofibers from Self-Assembling Pseudopeptide Building Blocks: Modulating the Handedness and Breaking the Helicity. *Small* **2008**, *4*, 1993–2005.
34. Chen, C. L.; Rosi, N. L. Peptide-Based Methods for the Preparation of Nanostructured Inorganic Materials. *Angew. Chem., Int. Ed.* **2010**, *49*, 1924–1942.
35. Sharma, J.; Chhabra, R.; Cheng, A.; Brownell, J.; Liu, Y.; Yan, H. Control of Self-Assembly of DNA Tubules Through Integration of Gold Nanoparticles. *Science* **2009**, *323*, 112–116.
36. Seddon, A. M.; Patel, H. M.; Burkett, S. L.; Mann, S. Chiral Templating of Silica-Lipid Lamellar Mesophase with Helical Tubular Architecture. *Angew. Chem., Int. Ed.* **2002**, *41*, 2988–2991.
37. Qiao, Y.; Lin, Y. Y.; Wang, Y. J.; Yang, Z. Y.; Liu, J.; Zhou, J.; Yan, Y.; Huang, J. B. Metal-Driven Hierarchical Self-Assembled One-Dimensional Nanohelices. *Nano Lett.* **2009**, *9*, 4500–4504.
38. Han, Y.; Zhao, L.; Ying, J. Y. Entropy-Driven Helical Mesostructure Formation with Achiral Cationic Surfactant Templates. *Adv. Mater.* **2007**, *19*, 2454–2459.
39. Orme, C. A.; Noy, A.; Wierzbicki, A.; McBride, M. T.; Grantham, M.; Teng, H. H.; Dove, P. M.; DeYoreo, J. J. Formation of Chiral Morphologies Through Selective Binding of Amino Acids to Calcite Surface Steps. *Nature* **2001**, *411*, 775–779.
40. Yu, S. H.; Colfen, H.; Tauer, K.; Antonietti, M. Tectonic Arrangement of $BaCO_3$ Nanocrystals into Helices Induced by A Racemic Block Copolymer. *Nat. Mater.* **2005**, *4*, 51–55.
41. Ye, H. M.; Wang, J. S.; Tang, S.; Xu, J.; Feng, X. Q.; Guo, B. H.; Xie, X. M.; Zhou, J. J.; Li, L.; Wu, Q.; *et al.* Surface Stress Effects on the Bending Direction and Twisting Chirality of Lamellar Crystals of Chiral Polymer. *Macromolecules* **2010**, *43*, 5762–5770.
42. Ye, H. M.; Xu, J.; Freudenthal, J.; Kahr, B. On the Circular Birefringence of Polycrystalline Polymers: Polylactide. *J. Am. Chem. Soc.* **2011**, *133*, 13848–13851.
43. Ding, F.; Harutyunyan, A. R.; Yakobson, B. I. Dislocation Theory of Chirality-Controlled Nanotube Growth. *Proc. Natl. Acad. Sci. U. S. A.* **2009**, *106*, 2506–2509.
44. Marchand, M.; Journet, C.; Guillot, D.; Benoit, J. M.; Yakobson, B. I.; Purcell, S. T. Growing a Carbon Nanotube Atom by Atom: "And Yet It Does Turn". *Nano Lett.* **2009**, *9*, 2961–2966.

45. Behr, M. J.; Mkhoyan, K. A.; Aydil, E. S. Catalyst Rotation, Twisting, and Bending during Multiwall Carbon Nanotube Growth. *Carbon* **2010**, *48*, 3840–3845.
46. Cervantes-Sodi, F.; Vilatela, J. J.; Jiménez-Rodríguez, J. A.; Reyes-Gutiérrez, L. G.; Rosas-Meléndez, S.; Íñiguez-Rábago, A.; Ballesteros-Villarreal, M.; Palacios, E.; Reiband, G.; Terrones, M. Carbon Nanotube Bundles Self-Assembled in Double Helix Microstructures. *Carbon* **2012**, 10.1016/j.carbon.2012.03.042.